Nucleic Acids Research, 2025, **53**, gkaf751
https://doi.org/10.1093/nar/gkaf751
Molecular and Structural Biology

Structural and functional characterization of CspR, a 2′-*O*-methyltransferase acting on wobble position within tRNA

Jaehun Yoo†, Yeji Lee†, Gyuhyeok Cho†, Jihyo Lim, Jungwook Kim*

Department of Chemistry, Gwangju Institute of Science and Technology, Gwangju 61005, Korea

*To whom correspondence should be addressed. Email: jwkim@gist.ac.kr
†Jaehun Yoo, Yeji Lee and Gyuhyeok Cho contributed equally to this work.

Abstract

Post-transcriptional modifications of transfer RNA (tRNA) are essential for maintaining decoding fidelity and tRNA stability. Among these, 2′-*O*-ribosyl methylation is particularly prominent in bacteria. In this study, we provide structural and biochemical evidence identifying CspR from *Bacillus subtilis* as an ortholog of *Escherichia coli* TrmL, which specifically methylates the 2′-*O*-ribose of the wobble position of $tRNA^{Leu}$(CAA), $tRNA^{Leu}$(UAA), and $tRNA^{Phe}$(GAA), in the presence of 2-methylthio-N^6-isopentenyladenosine at position 37 (ms^2i^6A37). X-ray crystal structures of CspR in complex with $tRNA^{Leu}$(UAA) and in its tRNA-free form reveal substantial conformational rearrangements upon tRNA binding. Notably, the tRNA-bound structure shows specific interactions between the anticodon loop and CspR's dimeric interface, with key residues U33, 5-carboxymethylaminomethyluridine34 ($cmnm^5U34$), and ms^2i^6A37 adopting flipped-out conformations. Furthermore, the structure uncovers extensive hydrophobic interactions between the isopentenyl group of ms^2i^6A37 and CspR, explaining the critical requirement of hypermodified A37 for enzymatic activity.

Graphical abstract

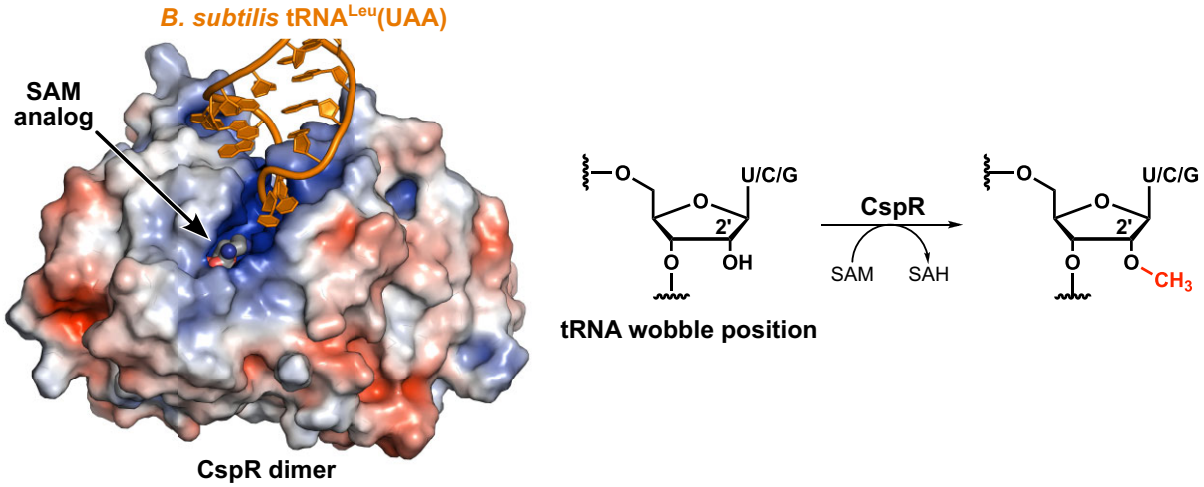

Introduction

RNA undergoes post-transcriptional modifications essential for its biological functions [1] with transfer RNA (tRNA) being the most extensively modified among all RNA classes [2]. tRNA plays a fundamental role in protein biosynthesis as an adaptor molecule by decoding nucleotide sequences in mRNA into corresponding amino acid during ribosomal translation [3]. Modifications of tRNA are most frequent within the anticodon stem loop (ASL) [4], particularly at positions 34 and 37, which house the anticodon triplet (positions 34, 35, and 36). Among various RNA modifications, methylation is the most conserved, identified in at least 73 nucleosides to date [5, 6]. This modification in the ASL enhances codon recognition accuracy and aids tRNA translocation from the ribosomal decoding site [4]. For instance, methylation of the 2′-hydroxy groups at the anticodon's first position stabilizes the codon–anticodon duplex [7]. The importance of this modification is underscored by observations in a yeast strain lacking *trm7*—responsible for 2′-*O*-ribose methylation at positions 32 and 34 of the ASL—which exhibited impaired translation [8].

In *E. coli* tRNA, three distinct 2′-*O*-methylated positions have been identified [6]. At the G18 within

Received: September 20, 2024. **Revised:** July 14, 2025. **Editorial Decision:** July 15, 2025. **Accepted:** July 21, 2025

D-loop TrmH converts guanosine to 2′-*O*-methylated guanosine (Gm), a modification commonly found in Gram-negative but not Gram-positive bacteria [9]. In the anticodon loop of *Escherichia coli* tRNA, 2′-*O*-methylcytidine (Cm) and 2′-*O*-methyluridine (Um) occur at position 32, while Cm and 5-carboxymethylaminomethyl-2′-*O*-methyl uridine ($cmnm^5Um$) are at position 34. TrmJ, which acts on various tRNA species including $tRNA^{Gln1}$(UUG), $tRNA^{Gln2}$(CUG), $tRNA^{Ser1}$(UGA), $tRNA^{fMet1}$(CAU), $tRNA^{fMet2}$(CAU), and $tRNA^{Trp1}$(CCA), catalyzes the formation of Cm32/Um32 [10–12]. Conversely, Cm34 in *E. coli* $tRNA^{Leu}$(CAA) and $cmnm^5Um34$ in $tRNA^{Leu}$(UAA) are synthesized by TrmL (Fig. 1) [13]. These tRNA-specific 2′-OH methyltransferases (MTases)—TrmH, TrmJ, and TrmL—are part of the SPOUT superfamily, distinct from the Rossman-fold MTases (RFMs) that most RNA MTases belong to [14, 15]. Crystallographic studies have revealed that SPOUT enzymes possess a unique topological knot conformation [10–12, 16–20]. Notably, most SPOUT members are involved in methylation of the 2′-OH group on RNA, including those modifying tRNA and rRNA such as RlmB (G2251 of 23S rRNA) [21] and RlmE (U2552 of 23S rRNA) [22]. However, certain members are known to modify nucleobase rather than the 2′-OH of ribose, like TrmD on G37 of tRNA [17] and RsmE on U1498 of 16S rRNA [23].

The crystal structures of TrmL from *Haemophilus influenza* [24] and *E. coli* [19] reveal that the enzyme exists in a dimeric state, with the dimer formation being crucial for tRNA recognition, as suggested by a tRNA-docking model [16, 19]. Biochemical analyses of *E. coli* TrmL have shown that 2-methylthio-N^6-isopentenyladenosine (ms^2i^6A37) at position 37 is vital for its methylating activity on C/U 34 of $tRNA^{Leu}$(CAA/UAA) isoacceptors [25]. This hypermodified adenosine is produced by MiaA, which adds the isopentenyl group to N6, and MiaB, which facilitates methylthiolation at C2 of A37. Interestingly, further studies revealed that the N^6-isopentenyladenosine (i^6A) modification by MiaA alone is sufficient for guiding TrmL in tRNA modification [25]. This prerequisite role of i^6A37 for ribose methylation at the wobble pyrimidine exemplifies a modification circuit that functionally couples positions 34 and 37 [26, 27]. Meanwhile, RiboMeth-Seq analysis identified four 2′-*O*-methylated nucleosides in *Bacillus subtilis* tRNAs: Gm34 in $tRNA^{Phe}$(GAA), Cm34 in $tRNA^{Leu}$(CAA), $cmnm^5Um34$ in $tRNA^{Leu}$(UAA), and U*m34 (a mixture of $cmnm^5s^2Um$, mnm^5s^2Um, and mnm^5Um) in $tRNA^{Gln}$(UUG) [28]. Although no specific enzymatic activity has been experimentally linked to these modifications, a homology search indicates that *B. subtilis* CspR is 45% identical to *E. coli* TrmL. Therefore, it remains unclear whether CspR alone is responsible for the 2′-hydroxyl methylation of all four wobble nucleotides in *B. subtilis*, or if other enzymes are involved.

In this study, we present experimental evidence supporting that *B. subtilis* CspR is an ortholog of TrmL. Moreover, we report two X-ray crystal structures of CspR: one complexed with $tRNA^{Leu}$ and sinefungin and the other with *S*-adenosyl-L-homocysteine (SAH) only. These structures reveal remarkable conformational changes in both tRNA and the protein upon binding with one another, providing novel insights into the substrate recognition and catalysis. Especially, the tRNA-bound structure illustrates the molecular basis for the requirement for N^6-isopentenyl modification at A37 of a cognate tRNA.

Materials and methods

Cloning, protein expression, and purification

The full-length *cspR* gene was amplified by polymerase chain reaction (PCR) from the genomic DNA of *B. subtilis* subsp. *subtilis* str.168 using the primers shown in Supplementary Table S1. The PCR product was inserted into the LIC-pLATE51 vector (Thermo Scientific) with an N-terminal His6-tag. After confirming the sequence of cloned genes (Macrogen, Korea), *E. coli* BL21(DE3) was transformed with the plasmid for expression. The cells were grown in Luria-Bertani (LB) medium containing 100 μg/ml ampicillin at 37°C until optical density at 600 nm (OD_{600}) reached 0.6–0.8. Overexpression was induced with 0.5 mM isopropyl β-D-1-thiogalactopyranoside (IPTG) at 20°C overnight, and the cells were harvested by centrifugation at 14 372 × *g* for 15 min. The pelleted cells were resuspended with a lysis buffer containing 20 mM HEPES (pH 7.5), 300 mM NaCl, and 1 mM dithiothreitol (DTT) and then lysed by sonication with 5 s pulse and 25 s rest for 30 min. The lysate was centrifuged at 21 672 × *g* for 30 min and the supernatants were filtered through a 0.2 μm pore size syringe filter before being applied to the His-Trap HP column (Cytiva). The column was equilibrated with a binding buffer [20 mM HEPES (pH 7.5), 500 mM NaCl, and 20 mM imidazole] and eluted with a linear gradient of imidazole (20–500 mM). The eluted fractions were analyzed by sodium dodecyl sulfate–polyacrylamide gel electrophoresis (SDS–PAGE). Further purification was performed by size exclusion chromatography (SEC) column (HiLoad 16/600 Superdex 75pg, Cytiva) pre-equilibrated with a buffer containing 20 mM HEPES (pH 7.5), and 150 mM NaCl. The purified protein was flash-frozen in liquid nitrogen and stored at −86°C. CspR mutants were generated by *in vivo* cloning [29] using the primers listed in Supplementary Table S1 and were expressed and purified using the same protocol as wild-type CspR.

The *miaA* gene was amplified through PCR using genomic DNA from *B. subtilis* subsp. *subtilis* str.168 using the primers shown in Supplementary Table S1. Subsequently, the PCR product was cloned into the LIC-pLATE51 vector (Thermo Scientific) and the plasmid was transformed into *E. coli* BL21(DE3) for expression. The procedures for purification of *B. subtilis* MiaA were identical to those for *B. subtilis* CspR.

In vivo transcription of tRNA

The plasmid pBSTNAV, containing the *lpp* promoter and *rrnC* terminator (Addgene, USA), was used as the tRNA expression vector [30–32]. The *B. subtilis leuZ* [$tRNA^{Leu}$(UAA)] gene was amplified by polymerase chain reaction from a synthetic DNA template (IDT, USA). The primers used are summarized in Supplementary Table S2. The pBSTNAV vector and the amplified PCR fragments were double digested in 37°C water bath for 2 h using the restriction enzymes EcoRI and HindIII following the manufacturer's instructions (Enzynomics, Korea). The digested products were purified by agarose gel electrophoresis. Ligation was performed using T4 ligase (Enzynomics, Korea) at room temperature for 4 h. The insertion of *leuZ* gene into the pBSTNAV vector was confirmed by DNA sequencing (Macrogen, Korea).

For overexpression of tRNA, *trmL*-deficient *E. coli* cells (NBRP, Japan) were transformed with the pBSTNAV-*leuZ* plasmid and cultured in LB medium containing 100 μg/ml ampicillin at 37°C for 24 h. Cells were collected by centrifuga-

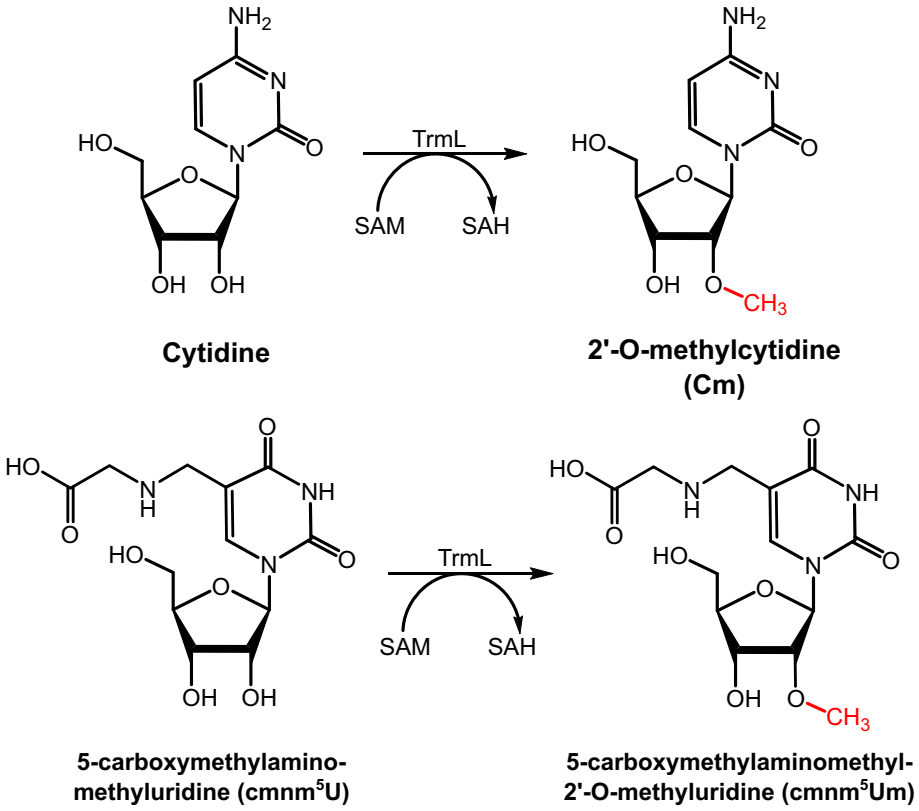

Figure 1. Chemical reaction catalyzed by TrmL. *E. coli* TrmL installs a methyl group on the 2′-hydroxyl of the wobble cytidine or uridine of $tRNA^{Leu}$. This activity is presumed to be performed by CspR in *B. subtilis*, where two enzymes share 45% sequence identity.

tion at 14 372 × *g* for 15 min and cellular RNA was extracted using 10 ml of saturated phenol (pH 4.5) per cells originating from 250 ml of LB culture (Biosesang, Korea). RNA precipitation was achieved by adding 0.1 volumes of 3 M sodium acetate (pH 5.3) and 3 volumes of isopropanol, respectively, to that of the phenol solution. The precipitated crude tRNA was transferred into a conical tube which was centrifuged at 14 372 × *g* for 15 min, followed by three 3 ml of washes of 75% (v/v) cold ethanol. RNA loading dye containing 0.025% (w/v) bromophenol blue and xylene cyanol FF in 95% (v/v) formamide was added to the RNA solution. The mixture was then applied to a 7 M urea-PAGE gel, which was run for 14 h at 40 W. The overexpressed $tRNA^{Leu}$(UAA) was resolved from endogenous tRNAs on the gel due to size differences. The band containing the desired tRNA was excised with a scalpel and tRNA was eluted from the gel strip using Elutrap Electroelution System (Whatman, U.K.). An extinction coefficient of $\varepsilon_{260} = 860\ 800\ M^{-1}\ cm^{-1}$ was used to quantify $tRNA^{Leu}$(UAA). Before use, the purified tRNA was denatured at 95°C for 5 min and then incubated on ice for 20 min.

Crystallization

To obtain the SAH-bound structure of *B. subtilis* CspR, we attempted to crystallize by sitting drop vapor diffusion method at room temperature. A mixture of 0.1 mM of *B. subtilis* CspR, 0.15 mM SAH, and 3 mM $MgCl_2$ in a buffer containing 20 mM MOPS (pH 7.0) and 150 mM NaCl was prepared. To this mixture, an equal volume (0.8 μL) of mother liquor was added. Crystals were obtained in a mother liquor composed of 0.2 M potassium sodium tartrate tetrahydrate, 0.1 M sodium citrate tribasic dihydrate (pH 5.6), and 0.2 M ammonium sulfate. The crystals were harvested using a nylon loop, cryo-protected by 20% glycerol (v/v), and flash-frozen in liquid nitrogen.

To obtain the tRNA-complexed structure of *B. subtilis* CspR, a mixture containing 0.04 mM *B. subtilis* CspR, 0.08 mM cellularly expressed $tRNA^{Leu}$ ($cmnm^5UAA$) extracted from *E. coli ΔtrmL* cells, and 0.5 mM sinefungin was prepared in a buffer with 25 mM HEPES (pH 7.5) and 150 mM NaCl. To this mixture, an equal volume (0.8 μl) of mother liquor was added. Crystals formed in a mother liquor composed of 0.1 M HEPES (pH 7.5) and 1.4 M sodium citrate tribasic dihydrate. The crystals were harvested using a nylon loop and flash-frozen in liquid nitrogen without cryoprotectant.

Data collection and structural determination

X-ray diffraction data were collected at the Pohang Accelerator Laboratory (PAL) beamline 7A (wavelength: 0.97934 Å) for SAH-bound CspR and beamline 5C (wavelength: 1.00003 Å) for tRNA-complexed CspR. For the SAH-bound structure, data were indexed, integrated, and scaled using XDS [33] and merged with Aimless [34] in the CCP4 suite [35]. For the tRNA-complexed structure, data were processed using Xia2 [36] with the DIALS-Aimless pipeline [34, 37], followed by anisotropic resolution cutoff using STARANISO [38]. To solve the phase problem for the SAH-bound CspR data, molecular replacement was performed with MOLREP [39], using the structure predicted by AlphaFold-2 (AF-O31590-F1) as a search model. For the tRNA-complexed CspR, SAH-bound CspR and tRNA from PDB ID:5ON2 were used to perform molecular replacement. Model build-

ing was performed using Coot [40] and refinement was conducted using REFMAC5 [41] and Phenix Refine [42]. Isotropic per-atom B-factors were refined without applying no translation/libration/screw (TLS) restraints [43]. To guide modeling of the homocysteine moiety of SAH, we referred to a high-resolution (1.50 Å) structure of a close ortholog from *B. anthracis* (PDB ID: 4PZK), which shares 70.5% sequence identity with *B. subtilis* CspR [44]. All structural visualizations were generated using PyMOL [45], and root mean square deviation (RMSD) values were calculated with align function of PyMOL using all heavy atoms.

Gene complementation assay

B. subtilis mutant strains, BKK08930 (*ΔcspR*), BKK17330 (*ΔmiaA*), and the parent strain *B. subtilis* 168 *trpC2*,1A1 were purchased from Bacillus Genetic Stock Center (BGSC). The *cspR* gene was cloned into a pHT01 vector (MoBiTec) by *in vivo* cloning [29]. The primers used for PCR are shown in Supplementary Table S1. The sequence of the plasmid containing *cspR* was verified by standard sequencing (Macrogen, Korea). For complementation assay, *B. subtilis ΔcspR* competent cells were transformed with the pHT01-*cspR* plasmid [46]. The transformed cells were grown in 1 L LB containing 5 μg/ml kanamycin and 5 μg/ml chloramphenicol at 37°C for 24 h. The harvested cell pellet was used for phenol extraction of bulk tRNA as described below. The extracted total tRNA from *B. subtilis* was hydrolyzed into nucleosides for analyses using high-performance liquid chromatography (HPLC) and liquid chromatography-mass spectrometry (LC-MS). The gene complementation assay for *ΔmiaA* was performed using the same method as used for *ΔcspR*.

Total tRNA extraction from *B. subtilis*

Cells were grown in 1 L LB containing 5 μg/ml kanamycin and 5 μg/ml chloramphenicol at 37°C for 24 h and harvested by centrifugation at 14 372 × *g* for 15 min. The pelleted cells were resuspended with 15 ml of buffer containing 0.3 M sodium acetate (pH 4.5), 10 mM EDTA, and 1 mg/ml of lysozyme then incubated at 37°C for 30 min. To extract cellular RNA, 16.7 ml of saturated phenol pH 4.5 (Biosesang) was added to the resuspended cells (for cells originating from 250 ml of LB culture) and incubated at 4°C for 30 min. After centrifugation, the aqueous layer was collected. To remove rRNA content, lithium chloride was added to the collected supernatant to a final concentration of 1 M using an 8 M stock solution, and incubated at 20°C overnight. The following precipitation, PAGE, and Elutrap was performed as described in "*In vivo* transcription of tRNA."

Purification of *B. subtilis* tRNA^{Phe}(GAA)

tRNA^{Phe}(GAA) was purified using a streptavidin affinity-based batch method as previously described [47–49]. A total of 18 mg of bulk *B. subtilis* wild-type tRNA, estimated to contain ∼25.4 nmol of tRNA^{Phe}(GAA), was dissolved in 60 × buffer B [30 mM HEPES-KOH (pH 7.5), 1.2 M NaCl, and 15 mM EDTA] supplemented with 0.5 mM DTT. A biotinylated DNA probe complementary to tRNA^{Phe}(GAA) (5′-CACGGATTTTCAGTCCGTTGCTCTACCAAC-3′; IDT, USA) was added at 1.875-fold molar excess, along with Streptavidin Sepharose High Performance affinity resin (Cytiva, USA) with 3.75-fold excess molar binding capacity. The mixture was incubated at 68°C for 10 min, then overnight at 4°C with gentle rocking. The resin was pelleted by centrifugation at 3214 × *g* for 5 min at 4°C, washed three times with 5× buffer B supplemented with 0.5 mM DTT, and the bound tRNA was eluted using 1× buffer B supplemented with 0.5 mM DTT at 68°C. The eluted RNA was precipitated with 70% (v/v) ethanol, separated on a 7 M urea-12% (w/v) PAGE gel, excised, and recovered by freeze–thaw extraction. For the *ΔcspR* strain, 26 mg of bulk RNA was used with the same protocol.

tRNA hydrolysis and HPLC/LC-MS analysis of nucleosides

The enriched *B. subtilis* bulk tRNA was denatured at 95°C for 5 min and then allowed to renature at room temperature. The sample was subsequently hydrolyzed into nucleosides by incubating in a solution containing buffer A (50 mM ammonium acetate (pH 6.0), 5 mM $ZnCl_2$, and 10 mM $MgCl_2$) with 1 U of Nuclease P1 (Sigma–Aldrich), 0.1 U of phosphodiesterase I (PDE I) (Sigma–Aldrich), and 1 U of Thermosensitive Alkaline Phosphatase (FastAP) (Thermo Scientific). The hydrolysis reaction was conducted at 37°C in a water bath for 15 h.

For HPLC analysis, 20 μl of the supernatant from the hydrolyzed samples was injected into an Agilent 1260 Infinity HPLC system equipped with a reversed-phase column (Agilent ZORBAX Eclipse Plus C18, 95 Å, 4.6 × 100 mm, 3.5 μm). The mobile phases consisted of solvent A (10 mM ammonium formate, pH 3.3) and solvent B (methanol). A stepped gradient was employed with a flow rate of 0.4 ml/min as follows: 2% solvent B for 8 min, 2%–50% solvent B for 8–32 min, 50% solvent B for 0.1 min, and 2% solvent B for 32.1–40 min. The diode array detector (DAD) wavelength was set to 272 nm, which is optimal for detecting 2′-O-methylcytidine. Nucleoside analysis of the bulk tRNA by HPLC was performed and the plots were generated using Origin 2022.

For LC-MS analysis, 20 μl of the hydrolyzed nucleosides were injected into an Elute UHPLC system (Bruker) coupled to an impact II QTOF mass spectrometer (Bruker) equipped with the same reversed-phase C18 column as above. The mobile phases consisted of solvent A [water with 0.1% (v/v) formic acid] and solvent B [acetonitrile with 0.1% (v/v) formic acid], and a gradient elution was performed at a flow rate of 0.4 ml/min as follows: 1%–12% B for 0–17.5 min, 12%–70% B for 17.5–20 min, 70% B for 20–25 min, and 1% B for 25–55 min. The electrospray ionization (ESI) parameters were set as follows: capillary voltage at 4500 V, end plate offset at 500 V, nebulizer at 4 bar, dry gas flow rate at 8 L/min, and dry temperature at 200°C. The ionized samples were analyzed in positive mode over a mass-to-charge ratio (*m*/*z*) range of 50–600 Da. The acquired data was processed using MZmine2 software [50].

Hydrolysis, *in vitro* reaction, and LC-MS analysis of tRNA^{Phe}(GAA)

For nucleoside analysis, 1 μg of purified *B. subtilis* tRNA^{Phe}(GAA) was denatured at 95°C for 5 min, renatured at room temperature, and hydrolyzed with 0.2 U Nuclease P1, 0.2 U PDE I, and 2 U FastAP in buffer A at 37°C for 2 h. For *in vitro* CspR assays, 1 μg of tRNA^{Phe}(GAA) from the *ΔcspR* strain was incubated with 10 μM recombinant CspR, 0.3 mM *S*-adenosyl-L-methionine (SAM), 1.25 mM NaOH, and 5 mM DTT in reaction buffer [20 mM HEPES (pH 7.5),

150 mM NaCl, and 10 mM $MgCl_2$] at 37°C for 11 h prior to hydrolysis as above.

Hydrolyzed nucleosides were analyzed using a Vanquish Flex UHPLC system (Thermo Scientific) coupled to an Orbitrap Exploris 120 mass spectrometer (Thermo Scientific), using the same C18 column and LC gradient as the QTOF experiment. The heated ESI (H-ESI) source was operated in positive mode at 3500 V, scanning m/z 100–600. The ESI parameters were sheath gas 40 arb., auxiliary gas 10 arb., sweep gas 1 arb., ion transfer tube temperature 275°C, and vaporizer temperature 300°C. MS/MS fragmentation was performed at a collision energy of 30%. Raw data were converted using msConvert [51] and analyzed with MZmine v4.7.3 [50]. Graphs were visualized using SciDAVis v2.7.1.

In vitro transcription of $tRNA^{Leu}$(CAA)

In vitro transcription of *B. subtilis* $tRNA^{Leu}$(CAA) was performed utilizing T7 RNA polymerase reaction. The DNA templates, comprising both sense and antisense strands, were purchased from Integrated DNA Technologies (USA) and included the T7 promoter sequence upstream of the tRNA sequence. The sequence details of these DNA templates can be found in Supplementary Table S3. The sense and antisense DNA templates were purified by gel electrophoresis in a gel containing 7 M urea and 12% (w/v) acrylamide. For the transcription reaction, 40 μg/ml T7 RNA polymerase was added to a mixture containing 40 mM Tris–HCl (pH 8.0), 1 mM spermidine, 0.01% (v/v) Triton X-100, 2.5 mM DTT, 20 mM $MgCl_2$, and 1 μM DNA template. This mixture was incubated at 37°C for 6 h, after which the reaction was quenched with 0.5 M EDTA. The transcripts were precipitated with 3 M sodium acetate (pH 5.3) and ethanol at −20°C. The RNA pellet was dissolved in distilled water and further purified through gel electrophoresis employing a gel containing 7 M urea and 12% (w/v) acrylamide. The tRNA was eluted from the gel slice using Elutrap (Whatman), precipitated, and subjected to three washes with cold 70% (v/v) ethanol.

In vitro methylation assay of CspR coupled with MiaA-dependent isopentenylation

The reaction was initiated by adding 10 μM of *B. subtilis* CspR and MiaA to a reaction mixture composed of 25 mM HEPES (pH 7.5), 150 mM NaCl, 300 μM SAM, 300 μM dimethylallyl pyrophosphate (DMAPP), 4 mM $MgCl_2$, 5 mM DTT, and 50 μM $tRNA^{Leu}$(CAA). The mixture was incubated at 37°C in a water bath for 24 h. To stop the reaction, the mixture was heated to 95°C for 5 min. For analysis using LC-MS, the tRNA was hydrolyzed into nucleosides by adding Nuclease P1, phosphodiesterase, and FastAP enzymes. The mixture was then incubated at 37°C for 22 h.

In vitro methylation assay of CspR mutants

To assess the methyltransferase activity of CspR variants, *in vitro* assays were performed using *B. subtilis* $tRNA^{Leu}$(UAA) expressed in *E. coli ΔtrmL* as the substrate. Each 25 μl of reaction mixture contained 5 μM of either wild-type or mutant CspR, 50 μM $tRNA^{Leu}$(UAA), and 100 μM SAM in a buffer composed of 25 mM HEPES (pH 7.5) and 150 mM NaCl. Reactions were carried out at 20°C for 4 h and quenched by the addition of formic acid to a final concentration of 0.05% (v/v). The quenched mixtures were centrifuged at 21 672 × *g* for 10 s at 20°C, and 20 μl of the resulting supernatant was injected into a ZIC-HILIC column (200 Å, 4.6 × 150 mm, 5 μm; Merck, Germany) for HPLC analysis. The mobile phases consisted of solvent A (5 mM ammonium formate, pH 3.3) and solvent B (90:10, v/v, acetonitrile:50 mM ammonium formate, pH 3.3). A stepped gradient was applied at a flow rate of 1 ml/min as follows: 100% solvent B for 0–8 min; 100%–40% solvent B from 8 to 20 min; 0% solvent B from 20.1 to 25 min; and re-equilibration with 100% solvent B from 25.1 to 35 min. Absorbance was monitored at 260 nm using DAD. Peak areas corresponding to SAH and SAM were quantified, and the conversion rate was calculated as [SAH]/([SAH] + [SAM]). All assays were performed in triplicate, and the mean ± standard deviation was reported. Relative activity was expressed as a percentage of wild-type activity (set to 100%) and visualized as a bar graph using SciDAVis v.2.7.1.

Results

Gene complementation confirms the CspR-dependent formation of wobble Cm and $cmnm^5um$ on *B. subtilis* tRNA

It is predicted that *B. subtilis* CspR is a likely ortholog of *E. coli* TrmL, sharing 45% sequence identity. To test whether CspR functions as a tRNA 2′-*O*-methyltransferase in *B. subtilis*, gene complementation assays were carried out by transforming a *cspR*-deletion mutant of *B. subtilis* (*ΔcspR*) with a plasmid containing *cspR* gene. Total tRNA was enriched from the RNA pool of the *ΔcspR* cells using gel purification to remove rRNA contamination, which also includes 2′-*O*-methylated nucleoside like Cm, Um, and Gm [5]. After hydrolysis, the composition of the tRNA was analyzed by HPLC and LC-MS. The results revealed that Cm was undetectable in the purified total tRNA sample from *ΔcspR* transformed with an empty vector. However, the formation of the Cm was restored when the *cspR*-null mutant was transformed using the plasmid harboring *cspR*, as confirmed by HPLC analysis (Fig. 2A). Moreover, the results were corroborated by LC-MS analyses. Commercially available Cm was used as a reference standard (Fig. 2B and Supplementary Fig. S1A). The MS peak corresponding to Cm ($C_{10}H_{16}N_3O_5$; calculated $m/z = 258.1090$, observed $m/z = 258.1090$) was detected in the tRNA sample from the *ΔcspR* cells complemented with the *cspR*-containing plasmid, with an elution time similar that of the Cm standard (Fig. 2B and C).

Similarly, we were able to detect $cmnm^5Um$ in both the wild-type and *cspR*-complemented mutant strain via LC-MS analyses, but not in *ΔcspR* cells, with the observed m/z of 346.1275 ($C_{13}H_{20}N_3O_8$; calculated $m/z = 346.1250$) (Fig. 2D and E) and its fragment ions $cmnm^5$-uracil ($C_7H_{10}N_3O_4$; calculated $m/z = 200.0671$, observed $m/z = 200.0679$) and 2′-*O*-methylribose ($C_6H_{11}O_4$; calculated $m/z = 147.0657$, observed $m/z = 147.0661$) (Supplementary Fig. S1B). In contrast, Gm could not be confidently identified due to interference from other molecules with similar m/z values and overlapping elution times. Additionally, 2′-*O*-methylated $tRNA^{Gln}$(UUG) modifications such as U*m ($cmnm^5s^2Um$, mnm^5s^2Um, and mnm^5Um) were not detected, likely due to low abundance or insufficient signal in the total tRNA sample under our experimental conditions, in contrast to a previous report [28].

To investigate whether MiaA activity is the prerequisite for CspR as shown with *E. coli* TrmL, we conducted gene

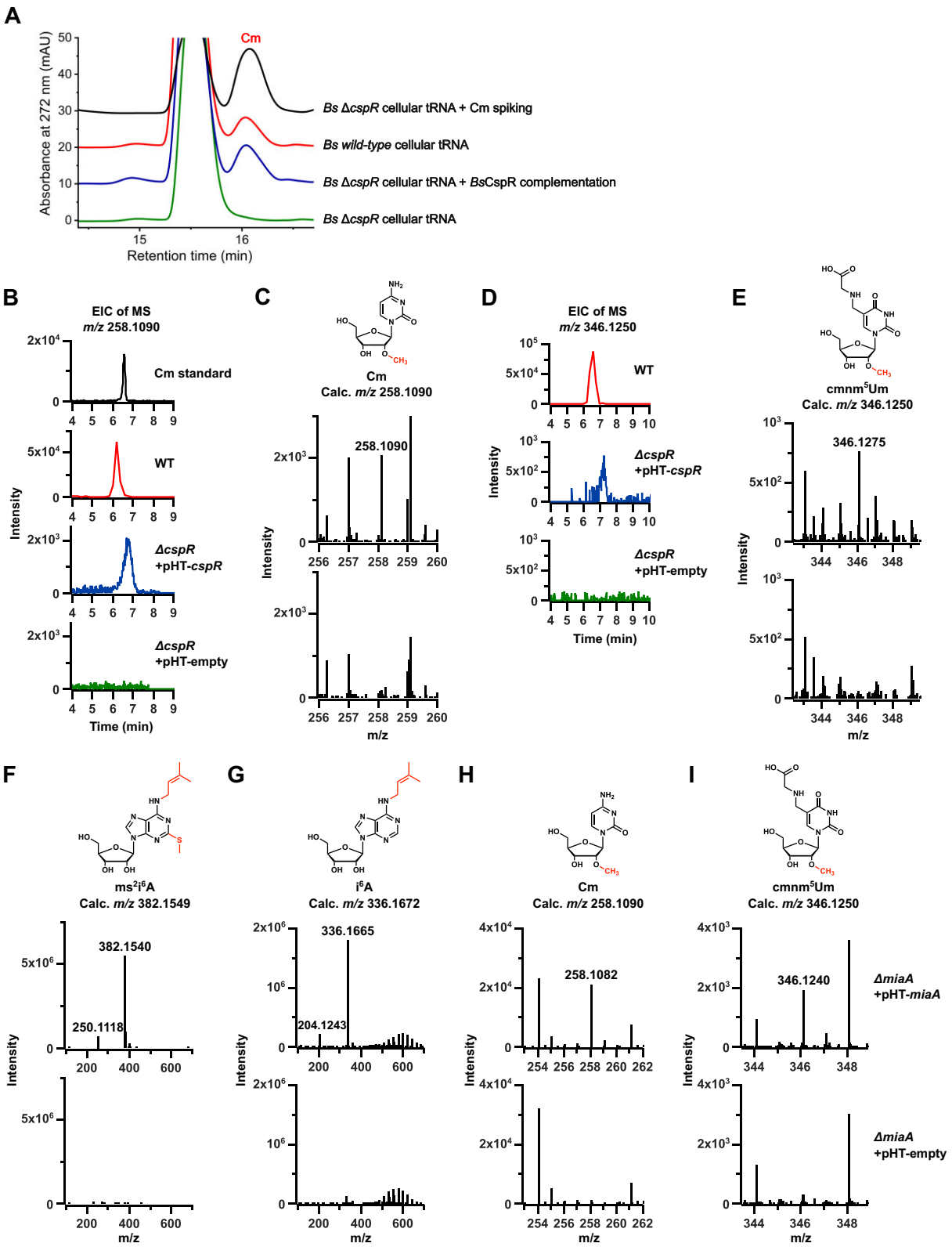

Figure 2. Gene complementation assay of *B. subtilis* Δ*cspR* and Δ*miaA*. (**A**) HPLC analysis verifying the presence of Cm (2′-*O*-methylcytidine) in total tRNA extracted from Δ*cspR*, Δ*cspR* complemented with a plasmid harboring the *cspR* gene, and the wild-type (WT) strain. A reference Cm standard, which eluted at ∼16 min, was spiked with the tRNA sample isolated from Δ*cspR* cells for comparison. (**B** and **C**) LC-MS analysis confirming the formation of Cm ($C_{10}H_{16}N_3O_5$; calculated $m/z = 258.1090$) in the Δ*cspR* strain complemented with the pHT-*Bs-cspR* plasmid. (B) Extracted ion chromatogram (EIC) and (C) corresponding MS spectra showing the Δ*cspR* strain (bottom panel) and the complemented strain (top panel). For the reference, Cm standard was compared. (**D** and **E**) LC-MS analysis confirming the formation of cmnm^{5}Um ($C_{13}H_{20}N_3O_8$; calculated $m/z = 346.1250$) in the same strains, shown as (D) EIC and (E) MS spectra. (**F–I**) LC-MS analysis of total tRNA extracted from the Δ*miaA* strain (bottom panels) and the strain complemented with pHT-*miaA* plasmid (top panels), verifying the presence of (F) ms^{2}i^{6}A ($C_{16}H_{24}N_5O_4S$; calculated $m/z = 382.1549$), (G) i^{6}A ($C_{15}H_{22}N_5O_4$; calculated $m/z = 336.1672$), (H) Cm, and (I) cmnm^{5}Um.

complementation assays using a *miaA*-deficient strain. Similar to *cspR*-complementation experiments, total tRNAs from *ΔmiaA* cells transformed with either an empty or a *miaA*-containing plasmid were extracted and examined by LC-MS analysis after hydrolysis. Interestingly, MS peaks corresponding to ms^2i^6A ($C_{16}H_{24}N_5O_4S$; calculated $m/z = 382.1549$, observed $m/z = 382.1540$), i^6A ($C_{15}H_{22}N_5O_4$; calculated $m/z = 336.1672$, observed $m/z = 336.1665$), Cm (observed $m/z = 258.1082$), and $cmnm^5Um$ (observed $m/z = 346.1240$) (Fig. 2F–I) were restored in the *miaA*-complemented mutant cells, whereas neither was detected in the *ΔmiaA* strain. The result confirms that analogous to *E. coli* TrmL, CspR requires MiaA for its 2′-*O*-methylation activity in cells [13].

In vitro methyl transfer assay of CspR

We first validated the *in vitro* activity of CspR toward hypermodified tRNAs. We employed cellularly derived tRNA containing ms^2i^6A37 modification. We were able to purify *B. subtilis* $tRNA^{Leu}$(UAA) expressed in *E. coli ΔtrmL* strain to near homogeneity [30–32], which contains an unusually long variable loop, enabling size-based separation via polyacrylamide gel electrophoresis [52]. Due to expression of the tRNA from *trmL*-deficient mutant cells, it contains the required modification at A37 but lacks a methyl group on the ribose of $cmnm^5U34$ (Fig. 3A and B). Upon incubation with purified CspR, formation of $cmnm^5Um$ was confirmed by LC-MS (observed $m/z = 346.1261$) and further validated by MS/MS analysis of fragment ions (Fig. 3B and Supplementary Fig. S1C).

To assess the substrate specificity of CspR, we examined whether *E. coli* $tRNA^{Leu}$(UAA) could also serve as a substrate. The *B. subtilis* and *E. coli* $tRNA^{Leu}$(UAA) share 72% sequence identity (64 of 89 nucleotides). The *E. coli* $tRNA^{Leu}$(UAA), purified from the *E. coli ΔtrmL* strain, contains expected modifications including 4-thiouridine (s^4U), Gm, ms^2i^6A, and 5-methyluridine (m^5U), but lacks $cmnm^5Um$ (Supplementary Fig. S1D and E) [6]. When incubated with CspR, $cmnm^5Um$ formation was observed ($m/z = 346.1235$), with a fragmentation pattern similar to that of the *B. subtilis* tRNA (Supplementary Fig. S1E and F), confirming that the enzyme can recognize and modify heterologous tRNA.

To investigate CspR-mediated Gm modification, we purified *B. subtilis* $tRNA^{Phe}$(GAA) from both *B. subtilis* wild-type and *ΔcspR* strains using a 3′-biotin-labeled complementary DNA probe [47, 48]. The wild-type tRNA was expected to carry modifications including dihydrouridine (D), m^5U, ms^2i^6A, and two methylated guanosines, Gm and 7-methylguanosine (m^7G) [6]. To identify the modified guanosines, standards of 1-methylguanosine (m^1G), 2-methylguanosine (m^2G), m^7G, and Gm were analyzed by LC-MS to determine their retention times and fragmentation patterns (Supplementary Fig. S2A–C). Using these standards, both Gm ($C_{11}H_{16}N_5O_5$; calculated $m/z = 298.1151$, observed $m/z = 298.1162$) and m^7G were confirmed in the wild-type tRNA sample, along with all other expected modifications (Fig. 3C–E and Supplementary Fig. S2D). In contrast, Gm was absent in the *ΔcspR* strain, indicating that CspR is required for Gm biosynthesis in $tRNA^{Phe}$(GAA). When the *ΔcspR*-derived tRNA was incubated with purified CspR, a time-dependent increase in Gm signal was observed, with a fragmentation pattern consistent with the Gm standard (Fig. 3E and F, and Supplementary Fig. S2E), demonstrating enzymatic restoration of the modification. Collectively, these results demonstrate that *B. subtilis* CspR functions as a 2′-*O*-methyltransferase that catalyzes the formation of $cmnm^5Um$ and Gm in hypermodified tRNAs.

Next, we tested whether CspR is also active on hypomodified tRNAs. We conducted *in vitro* methyl transfer assays using T7-RNA polymerase transcribed *B. subtilis* $tRNA^{Leu}$(CAA) as the substrate. However, the formation of Cm could not be detected (Fig. 3G and H). Given that *in vitro* transcribed tRNA lacks naturally occurring post-transcriptional modifications, we reasoned that the observed inactivity might be attributed to the absence of a prerequisite modification for CspR at A37 on the substrate tRNA. To address whether the isopentenylation of A37 could rescue the *in vitro* activity of CspR, we performed assays using T7-RNA polymerase transcribed tRNA that had been pre-treated with *B. subtilis* MiaA and DMAPP, the isopentenyl donor. As anticipated, the *in vitro* transcript containing i^6A37 (observed $m/z = 336.1666$) was able to support the formation of Cm (observed $m/z = 258.1090$) by CspR (Fig. 3G and H).

Similarly, we attempted to verify the formation of Gm in *B. subtilis* $tRNA^{Phe}$(GAA) using the *in vitro* transcript for the substrate as in with $tRNA^{Leu}$(CAA) described above. When the *in vitro* transcript missing i^6A37 was employed in the assay, no methylation was observed, as expected (Fig. 3I and J). In contrast, when the transcript was modified with i^6A37, Gm (observed m/z 298.1122) was detected in the CspR reaction mixture by LC-MS, with a fragmentation pattern similar to that of Gm standard (Fig. 3I and J, and Supplementary Fig. S2F). These results indicate that isopentenylation at A37 is the minimal prerequisite for the 2′-*O*-methyltransferase activity of CspR on hypomodified tRNAs, highlighting a modification circuit between positions 34 and 37, analogous to that observed in *E. coli* TrmL [26, 27].

Overall structure of CspR

Although a number of structures of TrmL are available, an experimental structure of *B. subtilis* CspR has not been reported. Moreover, no TrmL–tRNA complex structure has been published to date, which would be important to understand the molecular basis for tRNA recognition, including substrate specificity and the dependence on the post-transcriptional status at A37. To address this issue, we determined the X-ray crystal structure of CspR complexed with $tRNA^{Leu}$(UAA) expressed in *E. coli ΔtrmL* strain [30–32] and sinefungin, a structural analog of SAM, to a resolution of 3.18 Å (Fig. 4A). Because the $tRNA^{Leu}$(UAA) was produced in *E. coli*, it is expected to contain natural post-transcriptional modifications. Indeed, we were able to observe bulky substituents on U34 and A37 during refinement and modeled them accordingly (Supplementary Fig. S3). However, all other small-sized modifications are too subtle for our data and have not been included in the final model. In addition to the tRNA-bound form, we solved the structure of tRNA-free CspR bound with SAH, a reaction product, to a resolution of 1.85 Å (Fig. 4B). The crystallographic statistics are summarized in Table 1. The two structures exhibit an essentially identical dimeric conformation of the protein with an estimated dimer interface area of 1481 and 1370 $Å^2$ for the complex structure and the SAH-bound structure, respectively. The oligomerization state of CspR in solution was further confirmed by size exclusion chromatography (Supplementary Fig. S4). The enzyme is

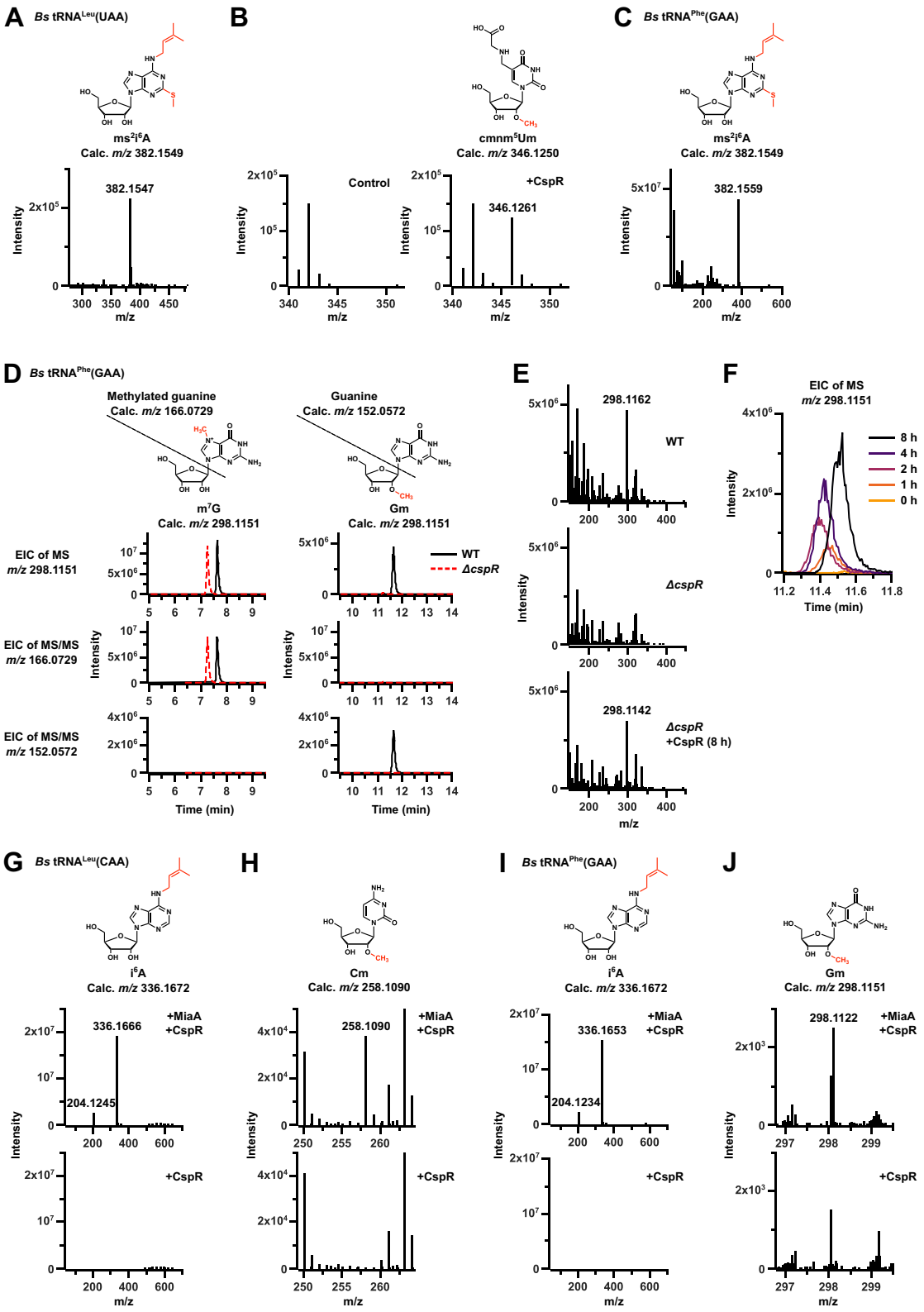

Figure 3. *In vitro* methyltransferase assay of *B. subtilis* CspR. (**A** and **B**) LC-MS analysis of *in vitro* CspR reactions using *B. subtilis* $tRNA^{Leu}$(UAA) extracted from *E. coli ΔtrmL*. (A) MS spectrum of ms^2i^6A from the $tRNA^{Leu}$(UAA) substrate. (B) MS spectra of $cmnm^5Um$ from reactions with (right) and without (left) CspR. (**C**–**F**) LC-MS analysis of *in vitro* CspR reactions using $tRNA^{Phe}$(GAA) extracted from *B. subtilis* WT and *ΔcspR*. (C) MS spectrum of ms^2i^6A from the $tRNA^{Phe}$(GAA) extracted from *ΔcspR*. (D) EIC of precursors and MS/MS fragment ions of m^7G and Gm ($C_{11}H_{16}N_5O_5$; calculated $m/z = 298.1151$) detected in samples from WT and *ΔcspR* strains. (E) MS spectra of Gm in WT, *ΔcspR*, and *ΔcspR* treated with CspR for 8 h. (F) Time-course analysis showing EICs of Gm, confirming the formation of Gm. (**G**–**J**) LC-MS analysis of *in vitro* reaction of MiaA and CspR using *in vitro* transcribed *B. subtilis* $tRNA^{Leu}$(CAA) (G and H) and $tRNA^{Phe}$(GAA) (I and J). MS spectra of (G and I) i^6A, (H) Cm, and (J) Gm from reactions with both MiaA and CspR (top panels) and with CspR alone (bottom panels).

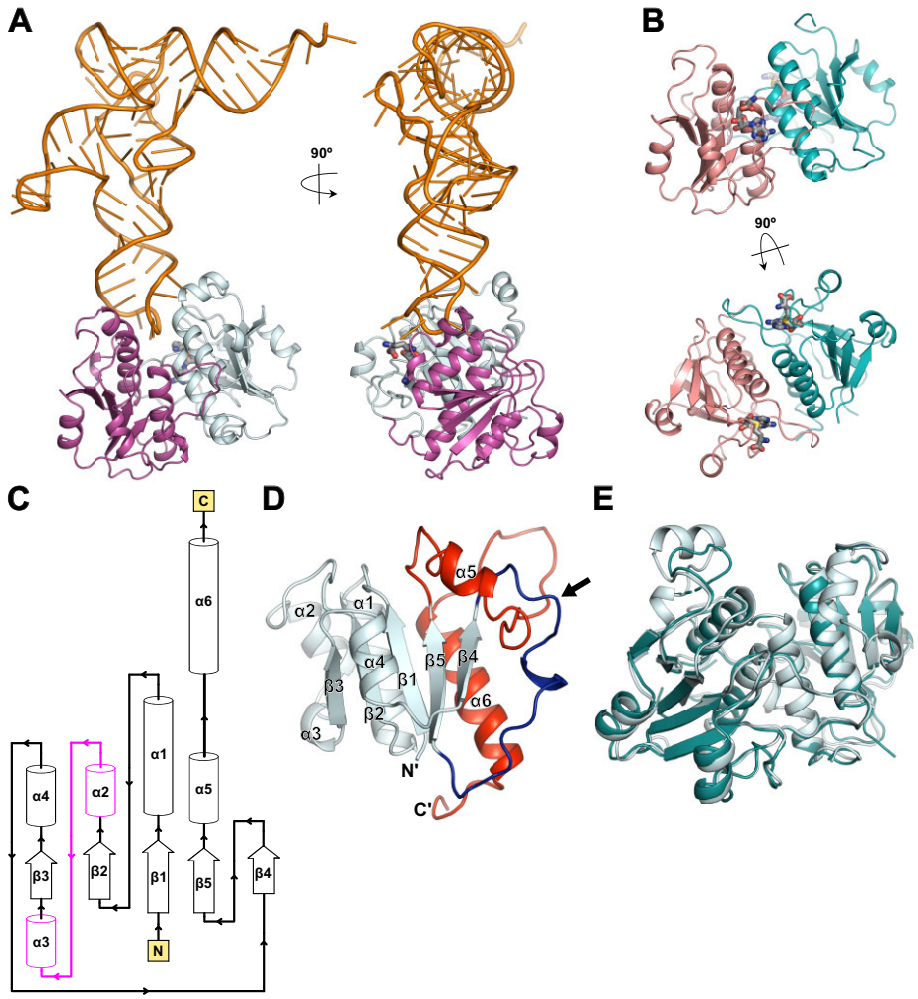

Figure 4. Overall structure of tRNA-complexed CspR and SAH-bound CspR. (**A**) The tRNA complexed structure of CspR where CspR (cyan and magenta) and tRNA (orange) are represented in cartoon. Sinefungin is represented in gray sticks. (**B**) The SAH-bound structure of CspR (salmon and teal). SAH is represented in gray sticks. Four sulfates and glycerol molecules were omitted for clarity. (**C**) The topology organization of CspR. The loop and helices from the SAH-bound CspR structure that were disordered are highlighted in magenta, which becomes visible in tRNA-complexed CspR structure. (**D**) The C-terminal region of the CspR adopts a distinctive knot fold, where crossing regions are colored in red (residues 107–160) and blue (residues 83–100), respectively. Knotted position is marked in a black arrow. (**E**) Superposition of SAH-bound CspR (teal) and tRNA complexed CspR (cyan). Teal dotted lines represent missing residues from 49 to 55.

composed of a sheet of five parallel β-strands, which is sandwiched by four α-helices arranged in the order β1-α1-β2-α2-α3-β3-α4-β4-β5-α5-α6. The topology organization of CspR is depicted in Fig. 4C. Notably, a knot is formed as the C-terminal residues (107–160) pass through a loop formed by residues 83–100 (Fig. 4D), which is a characteristic feature commonly observed in the SPOUT family. The structure of SAH-bound CspR closely aligns with that of *E. coli* TrmL (PDB ID: 4JAK), with an all-atom RMSD of only 0.786 Å (Supplementary Fig. S5). Superposition of SAH-bound CspR and tRNA complexed CspR exhibits an all-atom RMSD value of 0.894 Å (Fig. 4E). The most notable difference between the two structures is the loop and the helices in the complex structure which is disordered in the SAH-bound (Supplementary Fig. S6).

Interactions between CspR and $tRNA^{Leu}$(UAA)

In the asymmetric unit of the tRNA-bound structure, one CspR dimer and one $tRNA^{Leu}$(UAA) are found. Sinefungin is located in one subunit only (chain B), while the other subunit (chain C) is occupied by the 3′-end adenosine from a symmetry-related tRNA molecule instead (Supplementary Fig. S7). The tRNA binding occurs at the dimeric interface of CspR primarily through the anticodon loop domain encompassing U33-A37 (Fig. 5A and B). The anticodon loop adopts a unique conformation, where a total of four nucleobases are flipped out towards the solvent; i.e. U33, $cmnm^5U34$, A35, and ms^2i^6A37. Notably, the guanidinium group of Arg-135 forms a cation–π interaction with the nucleobase of U33, a hydrogen bond with the O4′ of the ribose, and is further stabilized via salt bridges with D54′ (Supplementary Fig. S8A). Furthermore, this arginine residue forms multiple hydrogen bonds with the O2, N3, and O4 of $cmnm^5U34$, thus playing a critical role in recognizing the U33–U34 pair (Fig. 5C). The O2 of wobble uridine forms an additional hydrogen bond with Tyr-55′ from the other subunit. The nitrogen of the 5-carboxymethylamino group forms ionic interaction with the backbone carbonyl group Thr-110. Ribose oxygens of $cmnm^5U34$ interact with Arg-24′ and its phos-

Table 1. Crystallographic statistics

	SAH-bound *Bs* CspR	$tRNA^{Leu}$(UAA)/ sinefungin-bound *B. subtilis* CspR
Data collection		
Wavelength (Å)	0.9793	1.0000
Space group	P_1	$P6_522$
Unit cell (*a*, *b*, *c*, α, β, γ) (Å, °)	39.76 46.96 50.09 110.33 92.71 106.56	136.83 136.83 184.11 90.00 90.00 120.00
Resolution range (Å)	39.20–1.85 (1.92–1.85)[a]	44.78–3.18 (3.35–3.18)[b]
R_{merge}	0.111 (0.977)	0.359 (6.62)
R_{meas}	0.130 (1.135)	0.364 (6.701)
$R_{p.i.m.}$	0.067 (0.578)	0.058 (1.023)
Total reflections	93 809 (5995)	566 332 (37 170)
Unique reflections	24 862 (1626)	14 622 (871)
Mean(I)/σ(I)	4.6 (1.3)	10.5 (1.0)
Completeness (%)	90.5 (58.8) (spherical)	82.6 (32.4) (spherical) 94.0 (61.3) (ellipsoidal)
Multiplicity	3.8 (3.7)	38.7 (42.7)
$CC_{1/2}$	0.993 (0.752)	0.994 (0.362)
Wilson B-factor ($Å^2$)	26.19	122.95
Refinement		
Resolution range	39.20–1.85 (1.92–1.85)	36.18–3.18 (3.30–3.18)
Reflections used in refinement	24 847 (1624)	14 605 (394)
Reflections used for free set	1279 (85)	767 (23)
R_{work}/R_{free}	0.195/0.238 (0.312/0.307)	0.216/0.252 (0.349/0.424)
Number of non-hydrogen atoms	2532	4512
Protein / tRNA	2343 / Not applicable	2567 / 1918
Ligands	78	27
Solvents	111	–
RMSD bonds (Å)	0.007	0.003
RMSD angles (°)	1.0	0.6
Ramachandran favored (%)	99.0	94.5
Ramachandran allowed (%)	1.0	5.2
Ramachandran outliers (%)	0.0	0.3
Average B-factor ($Å^2$)	31.3	106.2
Protein / tRNA	30.4 / Not applicable	97.5 / 117.9
Ligands	47.5	101.4
Solvents	39.5	–

[a]Numbers in parentheses refer to the highest-resolution shell.
[b]Anisotropic diffraction limits are 3.136 Å along 0.894 a* - 0.447 b*, 3.136 Å along b*, and 3.517 Å along c*, as determined by STARANISO.

phate group forms multiple salt bridges with Arg-50′. Meanwhile, the base of A35 penetrates deep into the cleft at the dimer interface and is engaged in a number of weak polar interactions with both protein protomers, including Asn-21, Asn-138, Asn-18′, Asn-138′, and Ser-140′ (Fig. 5D). Its phosphate group interacts with Asn-18 and Asn-138 via hydrogen bonds and forms a salt bridge with Arg-24′. The A36 base is stacked with that of A38, and its O2′ is stabilized by interactions with both the base of A38 and the phosphate group of ms^2i^6A37 (Supplementary Fig. S8B). The only interactions with the enzyme residue Arg-50′ occurs through its phosphate group. The adenine ring of ms^2i^6A37 forms hydrogen bonds via N3, N6, and N7 with Arg-50, the backbone carbonyl group and amine groups of Ser-42, respectively (Fig. 5E). Its O2′ contacts the backbone carbonyl group of Gly-40. Interestingly, the isopentenyl moiety of ms^2i^6A37 is embedded in a narrow groove formed by mostly hydrophobic residues, including Pro-16, Phe-41, Thr-43, Leu-48, Ala-51, Leu-53, and Trp-56. The 2-methylthio group does not appear to make a significant interaction with the enzyme nor tRNA molecule.

Of note, the residues Lys-49 to Tyr-55 in chain A and Asp-44 to Glu-57 in chain B are disordered due to conformational flexibility in the tRNA-free structure, which become fully ordered in both subunits of the tRNA-bound structure (Supplementary Fig. S6). While most of these residues in one protomer are engaged in non-polar interactions with ms^2i^6A37 as described above, the equivalent segment from the other protomer interacts with the phosphate backbones of $cmnm^5U34$ and A36 via salt bridge formation through Arg-50′ (Fig. 5B and Supplementary Fig. S8B). The restructuring of these residues in the tRNA-bound structure cannot be attributed to the crystal packing, since there is no symmetry related molecule in the vicinity, therefore supporting that these intermolecular interactions observed in our structure reflect a biological event.

Cofactor binding pocket

The binding site of SAH/sinefungin is near the knot structure in the C-terminus, near the dimeric interface. Both ligands display a similar binding pose in the pocket (Supplementary Fig. S9). Notably, the electron densities around the homocysteine group of SAH or sinefungin are relatively weaker compared to those of other parts of the cofactor probably due to conformational flexibility (Fig. 6A and B). The adenine and ribose moieties of the cofactor form multiple polar interactions mainly with backbone amide and carbonyl groups of the surrounding residues, as well as with side chains of Lys-84 and Met-130. The amine group of sinefungin, which is structurally equivalent to the *S*-methyl group of SAM, is ∼4.0 Å away from the 2′-OH of $cmnm^5U34$ (Fig. 7A). Notably, the ribose of the wobble uridine displays the 2′-endo pucker, maximizing the exposure of the 2′-hydroxyl group to the amine group of sinefungin.

Mutational analysis confirms key residues for CspR activity

To validate the interactions between CspR and tRNA observed in the crystal structures, we generated a series of alanine-substituted CspR mutants. The targeted residues included those involved in hydrogen bonding with the tRNA (Arg-24, Arg-50, Asp-54, Arg-135, and Asn-138) as well as one residue interacting with the cofactor base (Met-130). Although we attempted to purify an alanine mutant of Glu-109 to examine its potential role as a general base, the protein was poorly expressed and could not be obtained in sufficient quantity for enzymatic assays. Catalytic activity was evaluated by measuring the conversion of SAM to SAH using HPLC after a 4 h *in vitro* reaction (Supplementary Fig. S10 and Supplementary Table S4). All mutants exhibited significantly reduced activity (<25% of wild-type), confirming the functional importance of these residues in substrate recognition or catalysis. Specifically, the Arg-24-Ala mutant, which

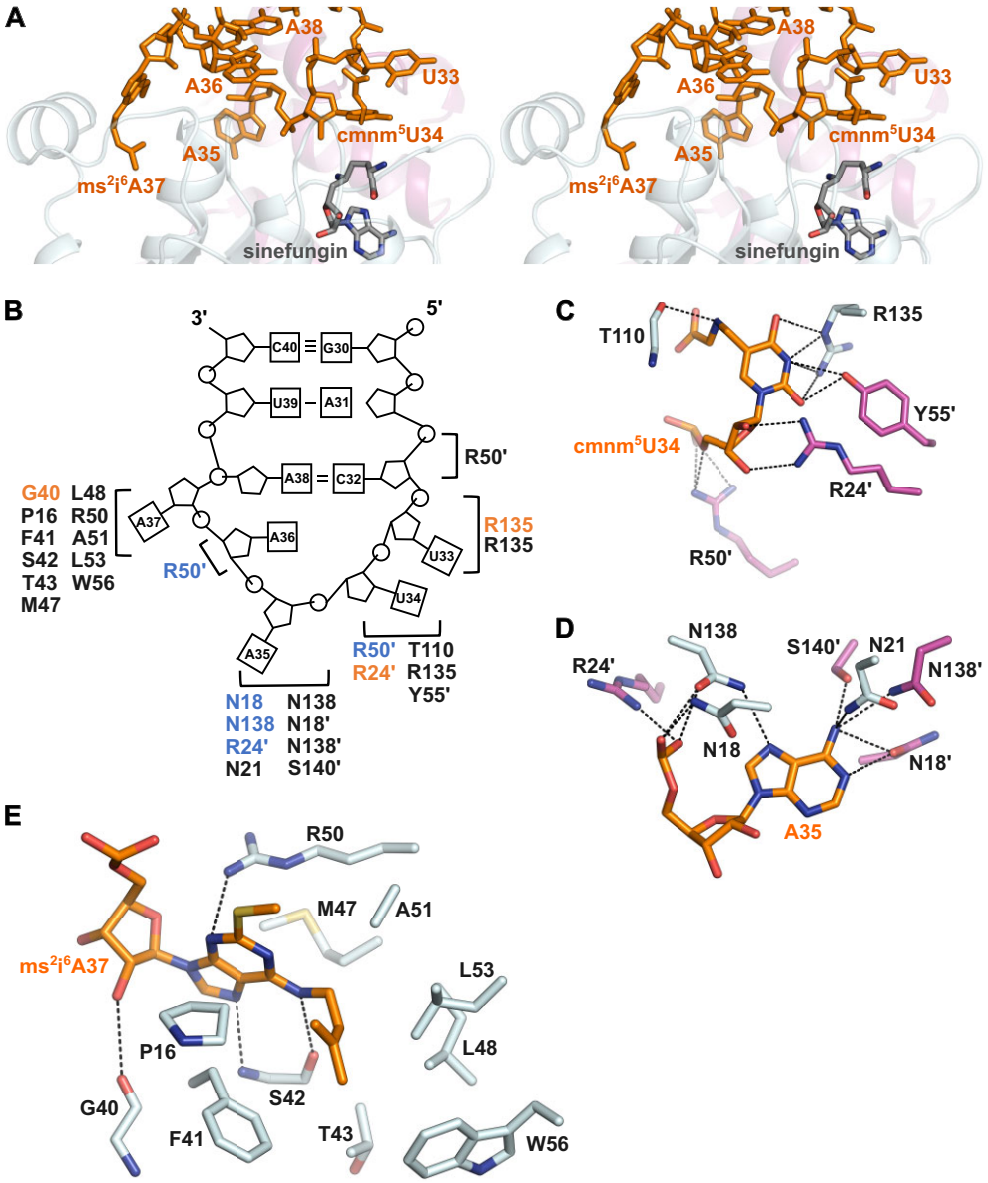

Figure 5. Interactions between CspR and tRNA^{Leu}(UAA). (**A**) Stereo view of the tRNA anticodon loop region (orange sticks) flipped out toward the active site of the CspR dimer (cyan and magenta cartoon). Sinefungin is shown as gray sticks. (**B**) Schematic diagram of tRNA residues that interacts with the CspR dimer interface. The phosphate group is represented as a circle, the ribose as a pentagon, and base as a square. Amino acids associated with the phosphate backbone (blue), ribose (orange), and base (black) are grouped in brackets for individual nucleotides. Protein residues from one protomer (chain B) are labeled without an apostrophe, while residues from the other protomer (chain C) are labeled with an apostrophe. (**C–E**) Amino acid residues contacting tRNA (C) cmnm^{5}U34, (D) A35, and (E) ms^{2}i^{6}A37. tRNA and interacting CspR residues are shown as sticks. Hydrogen bonds and salt bridges are indicated by black dashed lines.

disrupts hydrogen bonding with the 2′-OH of cmnm^{5}U34, retained only 17 ± 3% activity. The Arg-135-Ala mutant, responsible for base-specific recognition of U34, showed near-complete loss of activity (3.2%). Substitution of Asp-54, which forms stabilizing salt bridges with Arg-135, reduced activity to 22 ± 6%. Mutation of Arg-50, which contacts C32, cmnm^{5}U34, A36, and ms^{2}i^{6}A37, also led to a severe loss of activity (3.2%). The Asn-138-Ala mutant, which disrupts interactions with A35, retained only 2.2% activity. Finally, mutation of Met-130, which interacts with the cofactor base, reduced activity to 6.7%. These results collectively support the critical roles of these residues in tRNA recognition and catalysis by CspR.

Discussion

Scope of substrate specificity of CspR

Although CspR is speculated as the TrmL ortholog in *B. subtilis* due to a high sequence homology, its cellular and biochemical function has not been experimentally tested to date. In this report, we provide the supporting evidence based on gene complementation and biochemical studies along with structural characterization via X-ray crystallography. Previously, Illumina-based RiboMethSeq analyses unveiled that tRNA^{Phe}(GAA), tRNA^{Leu}(CAA), tRNA^{Leu}(UAA), and tRNA^{Gln}(UUG) contain 2′-OCH$_3$ at the wobble position in *B. subtilis* [28]. Through genetic and *in vitro* experiments, we were able to verify CspR-dependent formation

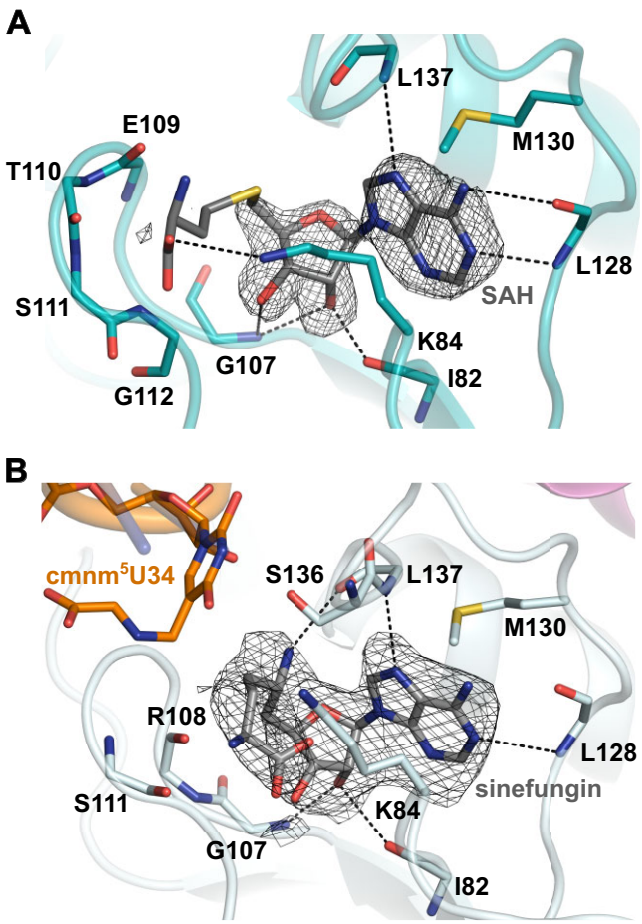

Figure 6. Cofactor binding pocket of CspR. (**A**) F_o-F_c omit map of the SAH-binding site contoured at 2.5 σ (black mesh), showing SAH (gray sticks) and surrounding amino acid residues (teal sticks). (**B**) F_o-F_c omit map of the sinefungin-binding site contoured at 2.5 σ (black mesh), showing sinefungin (gray sticks) and surrounding amino acid residues (cyan sticks). The cmnm^{5}U34 (orange sticks) from tRNA^{Leu}(UAA) is also shown. Hydrogen bonds and a salt bridge are indicated by black dashed lines.

of Cm in tRNA^{Leu}(CAA), cmnm^{5}Um in tRNA^{Leu}(UAA), and Gm in tRNA^{Phe}(GAA). Our assay results are in line with the necessity of isopentenylated A37 for 2′-O-methylation in tRNA substrates as previously observed with *E. coli* TrmL [13, 25]. The tRNA-bound structure provides detailed explanation for this observation, where the modified A37 promotes a tighter binding with the enzyme through intense hydrophobic interactions. The isopentenylated A37 (ms^{2}i^{6}A37) is deeply buried in a hydrophobic pocket formed by residues F41-W56. Upon tRNA binding, the previously disordered K49-Y55 loop adopts an ordered conformation and contributes to the hydrophobic environment, reinforcing enzyme–tRNA interaction. This disorder-to-order transition suggests that the ms^{2}i^{6}A37 modification promotes substrate binding by stabilizing the CspR–tRNA interface.

Notably, we were unable to detect CspR-dependent 2′-OH modification of tRNA^{Gln}(UUG) under both cellular and *in vitro* conditions. This isoacceptor, which contains G36-A37-C38, is not known or predicted to be modified by MiaA, which recognizes the specificity element of A36-A37-A38 in tRNA substrates. Given the essential role of the modified A37 in CspR activity, we conclude that tRNA^{Gln}(UUG) is not a substrate for CspR.

It has been reported that *E. coli* TrmL methylates 2′-OH of C34 and cmnm^{5}U34 of tRNA^{Leu}((C/U)AA) but not G34 in tRNA^{Phe}(GAA) [25]. Mutagenesis studies showed that replacing G34 with pyrimidine allowed TrmL to methylate the mutant tRNA^{Phe}, indicating that TrmL strictly recognizes pyrimidine, not purine, at the wobble position [13]. However, our data show that *B. subtilis* CspR can catalyze 2′-*O*-methylation at tRNA^{Phe}(GAA), which is somewhat puzzling considering a high sequence and structural homology between these two proteins (Supplementary Fig. S11). The broader specificity of CspR implies subtle yet functionally significant differences in substrate recognition, requiring future investigation into the structural determinants underlying this divergence.

Structural basis for substrate specificity of CspR

The present tRNA-bound structure of CspR reveals key insights into the enzyme's base specificity at the wobble position. The side chain of the essentially invariant (>99% conserved based on ConSurf [53]) Arg-135 forms multiple polar interactions with the O2, N3, and O4 of U34 in addition to cation–π interaction with U33. Further, the O2 of U34 forms an additional hydrogen bond with Tyr-55′. These complex intermolecular interactions would be still retained when the wobble position is replaced with cytidine, but not with guanosine. The guanidinium group of Arg-135 is precisely positioned around the flipped-out bases of U33 and U34 in the anticodon loop, stabilized by salt bridges with Asp-54′, another highly conserved residue (>95%) in CspR. Thus, in conjunction with ms^{2}i^{6}A37, C34/U34 serve as the primary determinants of substrate specificity for CspR. In the case of tRNA^{Phe}(GAA), which contains G34, we speculate that the less bulkier Hoogsteen edge of guanine may enable alternative interactions with Arg-135′, in contrast to the Watson–Crick edge used by pyrimidines. Determination of the CspR-tRNA^{Phe}(GAA) complex structure is warranted to unambiguously verify this hypothesis.

Structural comparison of tRNA 2′-OH methylases

Methylation of the 2′-OH group of ribose is a widespread RNA modification found in tRNA, ribosomal RNA (rRNA), small nuclear RNA (snRNA), and messenger RNA (mRNA) [54]. In *E. coli*, four tRNA-modifying enzymes—TrmH(Gm18) [55], TrmD(m^{1}G37) [56], TrmJ(Um32/Cm32) [10], and TrmL(Um34/Cm34) [13]—have been identified as members of the SPOUT superfamily. Each of these enzymes contains a conserved catalytic SPOUT domain of ∼150 amino acids [57]. Most SPOUT methyltransferases contain C-terminal or N-terminal extension domains for binding RNA substrates [58]. Unlike other SPOUT methyltransferases, TrmL lacks an extension domain and consists solely of the catalytic SPOUT domain [19]. The small size of the monomer almost necessitates the participation of both protomers within the homodimeric CspR for binding one tRNA molecule and subsequent methylation, which is clearly demonstrated by our tRNA-bound structure. In the CspR/TrmL dimer, one subunit is rotated ∼90 degrees relative to the other. This arrangement resembles the perpendicular dimer formed by

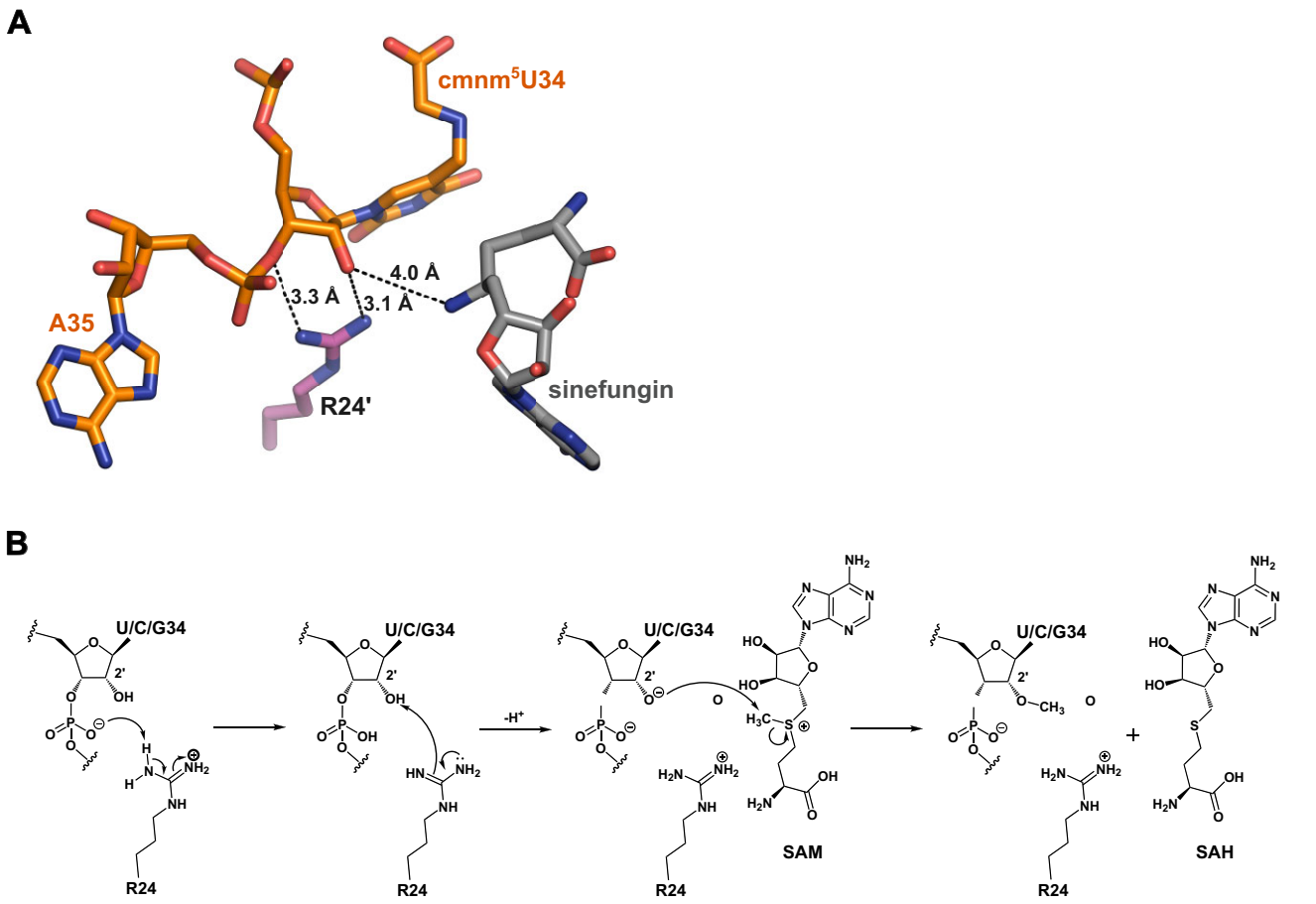

Figure 7. Proposed catalytic mechanism for SAM-dependent 2′-*O*-methylation of wobble uridine/cytidine/guanosine by CspR. (**A**) Close-up view of the CspR active site. Sinefungin is positioned facing the ribose of the wobble nucleotide. The amino group of sinefungin, which corresponds to the methyl group of SAM, lies 4.0 Å from the 2′-hydroxyl group of the cmnm^{5}U34 ribose (indicated by black dashed lines). Arg-24′ interacts with the O2′ and O3′ atoms of the ribose. (**B**) Schematic of the proposed catalytic mechanism. The phosphate group activates Arg-24′, enabling it to deprotonate the 2′-hydroxyl group of the wobble ribose. Subsequently, the oxyanion attacks the methyl group of SAM, forming U*m/Cm/Gm and SAH (*wobble uridine harbors further base modifications).

TrmH, while TrmD assembles in an antiparallel fashion [16, 17].

Proposed reaction mechanism of CspR

A previous study proposed Glu-103 as the general base for deprotonation of the 2′-OH in *T. thermophilus* TrmL [59], while Arg-41 plays a similar role in *T. thermophilus* TrmH, a Gm18 methyltransferase [16]. In our complex structure of CspR, Arg-24 is positioned 3.1 Å from the 2′-OH of cmnm^{5}U34 and forms a salt bridge with the tRNA phosphate backbone, making it the most likely candidate for the general base in the deprotonation step. Meanwhile, Glu-109, which corresponds to Glu-103 in *T. thermophilus* TrmL, is located 5.5 Å from the 2′-OH, making it less likely to serve as the primary general base. Given that the Arg-24-Ala mutant retains 17% of wild-type activity, it is plausible that Glu-109 may act as an auxiliary or compensatory general base during catalysis.

We propose a reaction mechanism for CspR, similar to that of Gm18 methylation by *T. thermophilus* TrmH [16] (Fig. 7B): The basicity of Arg-24 is enhanced by the anionic phosphate group of tRNA residue A35, facilitating deprotonation of the 2′-OH at the wobble position. The resulting nucleophilic oxyanion then attacks the methyl group of SAM, completing the methyl transfer.

Acknowledgements

We thank 5C and 7A beamlines of Pohang Accelerator Laboratory (PAL-5C, PAL-7A) in Pohang, South Korea, for their assistance on X-ray diffraction data collection. *E. coli* and *B. subtilis* strains were distributed by National BioResource Project (NBRP, Japan) or Bacillus Genetic Stock Center (BGSC, USA), respectively. We also acknowledge the GIST Advanced Institute of Instrumental Analysis (GAIA) for their support and service in mass spectrometry.

Author contributions: Jaehun Yoo (Conceptualization, Formal analysis, Investigation, Methodology, Visualization, Writing—original draft, Writing—review & editing), Yeji Lee (Conceptualization, Formal analysis, Investigation, Methodology, Visualization, Writing—original draft), Gyuhyeok Cho (Formal analysis, Investigation, Methodology, Visualization, Writing—review & editing), Jihyo Lim (Investigation), and Jungwook Kim (Conceptualization, Formal analysis, Funding acquisition, Methodology, Project administration, Resources, Supervision, Writing—original draft, Writing—review & editing).

Supplementary data

Supplementary data is available at NAR online.

Conflict of interest

The authors declare no conflicts of interest.

Funding

This work was supported by the National Research Foundation of Korea [2021R1A2C2009773, RS-2024-00411137, RS-2024-00440614]. Funding to pay the Open Access publication charges for this article was provided by the National Research Foundation of Korea [RS-2024-00440614].

Data availability

The atomic coordinates and structure factors for SAH-bound *B. subtilis* CspR and $tRNA^{Leu}$(UAA)/sinefungin-bound *B. subtilis* CspR are deposited to Protein Data Bank (PDB) under accession code 8W9U and 9J5P, respectively.

References

1. El Yacoubi B, Bailly M, De Crécy-Lagard V. Biosynthesis and function of posttranscriptional modifications of transfer RNAs. *Annu Rev Genet* 2012;**46**:69–95. https://doi.org/10.1146/annurev-genet-110711-155641
2. Hou YM, Perona JJ. Stereochemical mechanisms of tRNA methyltransferases. *FEBS Lett* 2010;**584**:278–86. https://doi.org/10.1016/j.febslet.2009.11.075
3. Zhou XL, Wang ED. Transfer RNA: a dancer between charging and mis-charging for protein biosynthesis. *Sci China Life Sci* 2013;**56**:921–32.
4. Agris PF. Bringing order to translation: the contributions of transfer RNA anticodon-domain modifications. *EMBO Rep* 2008;**9**:629–35. https://doi.org/10.1038/embor.2008.104
5. Motorin Y, Helm M. RNA nucleotide methylation: 2021 update nucleotide methylation: 2021 update. *WIREs RNA* 2022;**13**:e1691. https://doi.org/10.1002/wrna.1691
6. Cappannini A, Ray A, Purta E *et al.* MODOMICS: a database of RNA modifications and related information. 2023 update. *Nucleic Acids Res* 2024;**52**:D239–44. https://doi.org/10.1093/nar/gkad1083
7. Satoh A, Takai K, Ouchi R *et al.* Effects of anticodon 2′-*O*-methylations on tRNA codon recognition in an Escherichia coli cell-free translation. *RNA* 2000;**6**:680–6. https://doi.org/10.1017/S1355838200000029
8. Pintard L, Lecointe F, Bujnicki JM *et al.* Trm7p catalyses the formation of two 2′-*O*-methylriboses in yeast tRNA anticodon loop. *EMBO J* 2002;**21**:1811–20. https://doi.org/10.1093/emboj/21.7.1811
9. Persson B, Jäger G, Gustafsson C. The spoU gene of Escherichia coli, the fourth gene of the spoT operon, is essential for tRNA (Gm18) 2′-*O*-methyltransferase activity. *Nucleic Acids Res* 1997;**25**:4093–7. https://doi.org/10.1093/nar/25.20.4093
10. Purta E, van Vliet F, Tkaczuk KL *et al.* The yfhQ gene of *Escherichia coli* encodes a tRNA:cm32/Um32 methyltransferase. *BMC Mol Biol* 2006;**7**:23. https://doi.org/10.1186/1471-2199-7-23
11. Somme J, Van Laer B, Roovers M *et al.* Characterization of two homologous 2′-*O*-methyltransferases showing different specificities for their tRNA substrates. *RNA* 2014;**20**:1257–71. https://doi.org/10.1261/rna.044503.114
12. Liu RJ, Long T, Zhou M *et al.* TRNA recognition by a bacterial tRNA Xm32 modification enzyme from the SPOUT methyltransferase superfamily. *Nucleic Acids Res* 2015;**43**:7489–503. https://doi.org/10.1093/nar/gkv745
13. Benítez-Páez A, Villarroya M, Douthwaite S *et al.* YibK is the 2′-*O*-methyltransferase TrmL that modifies the wobble nucleotide in *Escherichia coli* $tRNA^{Leu}$ isoacceptors. *RNA* 2010;**16**:2131–43.
14. Martin JL, McMillan FM. SAM (dependent) I AM: the *S*-adenosylmethionine-dependent methyltransferase fold. *Curr Opin Struct Biol* 2002;**12**:783–93. https://doi.org/10.1016/S0959-440X(02)00391-3
15. Strassler SE, Bowles IE, Dey D *et al.* Tied up in knots: untangling substrate recognition by the SPOUT methyltransferases. *J Biol Chem* 2022;**298**:102393.https://doi.org/10.1016/j.jbc.2022.102393
16. Nureki O, Watanabe K, Fukai S *et al.* Deep knot structure for construction of active site and cofactor binding site of tRNA modification enzyme. *Structure* 2004;**12**:593–602. https://doi.org/10.1016/j.str.2004.03.003
17. Elkins PA, Watts JM, Zalacain M *et al.* Insights into catalysis by a knotted TrmD tRNA methyltransferase. *J Mol Biol* 2003;**333**:931–49. https://doi.org/10.1016/j.jmb.2003.09.011
18. Jaroensuk J, Atichartpongkul S, Chionh YH *et al.* Methylation at position 32 of tRNA catalyzed by TrmJ alters oxidative stress response in *Pseudomonas aeruginosa*. *Nucleic Acids Res* 2016;**44**:10834–48. https://doi.org/10.1093/nar/gkw870
19. Liu RJ, Zhou M, Fang ZP *et al.* The tRNA recognition mechanism of the minimalist SPOUT methyltransferase, TrmL. *Nucleic Acids Res* 2013;**41**:7828–42. https://doi.org/10.1093/nar/gkt568
20. Watanabe K, Nureki O, Fukai S *et al.* Roles of conserved amino acid sequence motifs in the SpoU (TrmH) RNA methyltransferase family. *J Biol Chem* 2005;**280**:10368–77. https://doi.org/10.1074/jbc.M411209200
21. Michel G, Sauvé V, Larocque R *et al.* The structure of the RlmB 23S rRNA methyltransferase reveals a new methyltransferase fold with a unique knot. *Structure* 2002;**10**:1303–15. https://doi.org/10.1016/S0969-2126(02)00852-3
22. Hager J, Staker BL, Jakob U. Substrate binding analysis of the 23S rRNA methyltransferase RrmJ. *J Bacteriol* 2004;**186**:6634–42. https://doi.org/10.1128/JB.186.19.6634-6642.2004
23. Basturea GN, Rudd KE, Deutscher MP. Identification and characterization of RsmE, the founding member of a new RNA base methyltransferase family. *RNA* 2006;**12**:426–34. https://doi.org/10.1261/rna.2283106
24. Lim K, Zhang H, Tempczyk A *et al.* Structure of the YibK methyltransferase from *Haemophilus influenzae* (HI0766): a cofactor bound at a site formed by a knot. *Proteins* 2003;**51**:56–67. https://doi.org/10.1002/prot.10323
25. Zhou M, Long T, Fang Z-P *et al.* Identification of determinants for tRNA substrate recognition by *Escherichia coli* C/U34 2′-*O*-methyltransferase. *RNA Biology* 2015;**12**:900–11. https://doi.org/10.1080/15476286.2015.1050576
26. Han L, Phizicky EM. A rationale for tRNA modification circuits in the anticodon loop. *RNA* 2018;**24**:1277–84. https://doi.org/10.1261/rna.067736.118
27. Barraud P, Tisné C. To be or not to be modified: miscellaneous aspects influencing nucleotide modifications in tRNAs. *IUBMB Life* 2019;**71**:1126–40. https://doi.org/10.1002/iub.2041
28. De Crécy-Lagard V, Ross R, Jaroch M *et al.* Survey and validation of tRNA modifications and their corresponding genes in *Bacillus subtilis* sp subtilis strain 168. *Biomolecules* 2020;**10**:977. https://doi.org/10.3390/biom10070977
29. Watson JF, García-Nafría J. *In vivo* DNA assembly using common laboratory bacteria: a re-emerging tool to simplify molecular cloning. *J Biol Chem* 2019;**294**:15271–81. https://doi.org/10.1074/jbc.REV119.009109
30. Ponchon L, Catala M, Seijo B *et al.* Co-expression of RNA–protein complexes in Escherichia coli and applications to RNA biology. *Nucleic Acids Res* 2013;**41**:e150. https://doi.org/10.1093/nar/gkt576
31. Ponchon L, Dardel F. Recombinant RNA technology: the tRNA scaffold. *Nat Methods* 2007;**4**:571–6. https://doi.org/10.1038/nmeth1058
32. Ponchon L, Beauvais G, Nonin-Lecomte S *et al.* A generic protocol for the expression and purification of recombinant RNA in *Escherichia coli* using a tRNA scaffold. *Nat Protoc* 2009;**4**:947–59. https://doi.org/10.1038/nprot.2009.67

33. Kabsch W. XDS. *Acta Crystallogr D Biol Crystallogr* 2010;**D66**:125–32. https://doi.org/10.1107/S0907444909047337
34. Evans PR, Murshudov GN. How good are my data and what is the resolution? *Acta Crystallogr D Biol Crystallogr* 2013;**69**:1204–14. https://doi.org/10.1107/S0907444913000061
35. Agirre J, Atanasova M, Bagdonas H *et al.* The *CCP* 4 suite: integrative software for macromolecular crystallography. *Acta Crystallogr D Struct Biol* 2023;**79**:449–61. https://doi.org/10.1107/S2059798323003595
36. Winter G. *xia2* : an expert system for macromolecular crystallography data reduction. *J Appl Crystallogr* 2010;**43**:186–90. https://doi.org/10.1107/S0021889809045701
37. Winter G, Waterman DG, Parkhurst JM *et al. DIALS* : implementation and evaluation of a new integration package. *Acta Crystallogr D Struct Biol* 2018;**74**:85–97. https://doi.org/10.1107/S2059798317017235
38. Tickle I, Flensburg C, Keller P. *et al. STARANISO*. Cambridge, United Kingdom: Global Phasing Ltd, 2018.
39. Vagin A, Teplyakov A. Molecular replacement with MOLREP. *Acta Crystallogr D Biol Crystallogr* 2010;**66**:22–5. https://doi.org/10.1107/S0907444909042589
40. Emsley P, Lohkamp B, Scott WG *et al.* Features and development of Coot. *Acta Crystallogr D Biol Crystallogr* 2010;**66**:486–501. https://doi.org/10.1107/S0907444910007493
41. Murshudov GN, Skubák P, Lebedev AA *et al.* REFMAC5 for the refinement of macromolecular crystal structures. *Acta Crystallogr D Biol Crystallogr* 2011;**67**:355–67. https://doi.org/10.1107/S0907444911001314
42. Afonine PV, Poon BK, Read RJ *et al.* Real-space refinement in PHENIX for cryo-EM and crystallography. *Acta Crystallogr D Struct Biol* 2018;**74**:531–44. https://doi.org/10.1107/S2059798318006551
43. Merritt EA. To *B* or not to *B* : a question of resolution? *Acta Crystallogr D Biol Crystallogr* 2012;**68**:468–77. https://doi.org/10.1107/S0907444911028320
44. Schubert HL, Blumenthal RM, Cheng X. Many paths to methyltransfer: a chronicle of convergence. *Trends Biochem Sci* 2003;**28**:329–35. https://doi.org/10.1016/S0968-0004(03)00090-2
45. Schrödinger, LLC The PyMOL Molecular Graphics System. https://www.pymol.org/ (29 July 2025, date lastaccessed).
46. Koo B-M, Kritikos G, Farelli JD *et al.* Construction and analysis of two genome-scale deletion libraries for *Bacillus subtilis*. *Cell Syst* 2017;**4**:291–305. https://doi.org/10.1016/j.cels.2016.12.013
47. Tsurui H, Kumazawa Y, Sanokawa R *et al.* Batchwise purification of specific tRNAs by a solid-phase DNA probe. *Anal Biochem* 1994;**221**:166–72. https://doi.org/10.1006/abio.1994.1393
48. Miyauchi K, Ohara T, Suzuki T. Automated parallel isolation of multiple species of non-coding RNAs by the reciprocal circulating chromatography method. *Nucleic Acids Res* 2007;**35**:e24. https://doi.org/10.1093/nar/gkl1129
49. Suzuki T, Suzuki T. Chaplet column chromatography: isolation of a large set of individual RNAs in a single step. In: *Methods in Enzymology*. Vol. **425**. Amsterdam, The Netherlands: Elsevier, 2007, 231–9.
50. Schmid R, Heuckeroth S, Korf A *et al.* Integrative analysis of multimodal mass spectrometry data in MZmine 3. *Nat Biotechnol* 2023;**41**:447–9. https://doi.org/10.1038/s41587-023-01690-2
51. Chambers MC, Maclean B, Burke R *et al.* A cross-platform toolkit for mass spectrometry and proteomics. *Nat Biotechnol* 2012;**30**:918–20. https://doi.org/10.1038/nbt.2377
52. Yoo J, Lee J, Kim J. Structural basis for the selective methylation of 5-carboxymethoxyuridine in tRNA modification. *Nucleic Acids Res* 2023;**51**:9432–41. https://doi.org/10.1093/nar/gkad668
53. Ashkenazy H, Abadi S, Martz E *et al.* ConSurf 2016: an improved methodology to estimate and visualize evolutionary conservation in macromolecules. *Nucleic Acids Res* 2016;**44**:W344–50. https://doi.org/10.1093/nar/gkw408
54. Ayadi L, Galvanin A, Pichot F *et al.* RNA ribose methylation (2′-O-methylation): occurrence, biosynthesis and biological functions. *Biochim Biophys Acta* 2019;**1862**:253–69. https://doi.org/10.1016/j.bbagrm.2018.11.009
55. Hori H, Suzuki T, Sugawara K *et al.* Identification and characterization of tRNA (Gm18) methyltransferase from *Thermus thermophilus* HB8: domain structure and conserved amino acid sequence motifs. *Genes Cells* 2002;**7**:259–72. https://doi.org/10.1046/j.1365-2443.2002.00520.x
56. Li J-N, Björk GR. Structural alterations of the tRNA(m1G37)methyltransferase from *Salmonella typhimurium* affect tRNA substrate specificity. *RNA* 1999;**5**:395–408. https://doi.org/10.1017/S1355838299980834
57. Hori H. Methylated nucleosides in tRNA and tRNA methyltransferases. *Front Genet* 2014;**5**:144. https://doi.org/10.3389/fgene.2014.00144
58. Toyooka T, Hori H. Differences in substrate selectivities of the SPOUT superfamily of methyltransferases. *Nucleic Acids Symp Ser* 2007;**51**:445–6. https://doi.org/10.1093/nass/nrm223
59. Pang P, Deng X, Wang Z *et al.* Structural and biochemical insights into the 2′-*O*-methylation of pyrimidines 34 in tRNA. *FEBS J* 2017;**284**:2251–63. https://doi.org/10.1111/febs.14120

Received: September 20, 2024. **Revised:** July 14, 2025. **Editorial Decision:** July 15, 2025. **Accepted:** July 21, 2025